Hydrology Research

Hydrology Research Vol 00 No 0, 1 doi: 10.2166/nh.2021.050

Application of red edge band in remote sensing extraction of surface water body: a case study based on GF-6 WFV data in arid area

Zhao Lu[a], Daqing Wang[a,*], Zhengdong Deng[a], Yue Shi[a], Zhibin Ding[a], Hao Ning[a], Hongfei Zhao[b], Jiazheng Zhao[c], Haoli Xu[a] and Xiaoning Zhao[a]

[a] Defense Engineering College, Army Engineering University, Nanjing 210007, China
[b] Postdoctoral Workstation of Jinling Hospital, Nanjing 210016, China
[c] Wuhu Environmental Supervision Detachment, Wuhu 241000, China
*Corresponding author. E-mail: wangdaqing2020@126.com

DW, 0000-0003-2470-4371

ABSTRACT

This paper mainly researches the application method of red edge band in water body remote sensing extraction. Gaofen-6 (GF-6) WFV data were chosen for the high spatial resolution, more bands, and wide width. Two new methods were proposed: the single-band threshold method based on the red edge 2 band and the decision tree model method based on the combined operation of the green band, red band, near infrared band, red edge 1 band, and red edge 2 band. Four traditional methods were used for comparing the extraction accuracy. Two study areas with different characteristics were chosen to analyze the reliability of the proposed method, one mountainous and one urban region, both located in Minqin, Gansu, China, which is a typical arid area. The results showed that the two red edge bands of the GF-6 WFV data can be utilized to extract water body information. Kappa coefficients extracted from the single-band threshold method based on the red edge 2 band in water bodies in mountainous and urban areas reached 96.18% and 93.21%, respectively. The decision tree method has the best extraction effect. Kappa coefficients of this method in mountain and urban water bodies were 97.73% and 94.41%, respectively.

Key words: decision tree, GF-6 WFV data, red edge band, surface water body extraction

HIGHLIGHTS

- The red edge band of Chinese Gaofen-6 WFV date was found to be applicable to the extraction of surface water.
- A decision tree model based on the joint operation of five bands was established, which can effectively extract surface water.

ABBREVIATIONS

AWEI	Automatic Water Extraction Index
CIWI	Combined Index of NVDI and NIR for Water Identification
EWI	Enhanced Water Index
FAI	Floating Algae Index
GF-6	GaoFen-6 satellite
ISODATA	Iterative Selforganizing Data Analysis Techniques algorithm
KNN	K-nearest neighbor
K-means	K-means clustering algorithm
MAWEI	Modified Automatic Water Extraction Index
MOWI	Modified Optimization Water Index
NDWI	Normalized Difference Water Index
NWI	New Water Body Index
PMS	Panchromatic/Multi-spectral cameras
PCA	Principal component analysis
SWI	Shadow Water Index
SVM	Support vector machine
WFV	Wide field view cameras

1. INTRODUCTION

As a very precious natural resource, surface water occupies a very important position in the ecological environment, directly affecting human production and life (Gong *et al.* 2018), especially the development of agriculture (Pierpaolo 2018). In arid and semi-arid areas where agriculture competes keenly with ecosystem for water, integrated management of both surface water and groundwater resources at basin scale is crucial (Wu *et al.* 2016). Therefore, accurately obtaining surface water information is very meaningful research. Remote sensing technology has the advantages of fast imaging, wide range, and short observation period. It can provide significant technical support for long-term, rapid and objective acquisition of surface water information. Extracting surface water information through remote sensing technology is currently one of the principal contents of remote sensing application research (Zhao *et al.* 2017).

Studies have shown that non-water features (such as terrain shadows, vegetation shadows, etc.) on remote sensing images affect the accuracy of water body extraction (Kasvi *et al.* 2019; Yue *et al.* 2020). In order to effectively extract real water bodies, researchers have proceeded to do a great deal of research and explore some methods (Bijeesh & Narasimhamurthy 2020). According to the characteristics of the extraction methods, these methods can fall into three types.

The first type of remote sensing extraction method is built on the spectral characteristics of water. This type of method mainly uses a single band or multiple bands in remote sensing images to construct models, which extracts water bodies by suppressing remote sensing information of non-water body features such as vegetation, buildings, and soil. Such methods include single-band threshold method (Liu *et al.* 2019), spectral relationship method (Zhang 2008), and so on. Water body indexes based on spectral characteristics have also been proposed and applied to water body extraction research, such as: Floating Algae Index (FAI) (Xu *et al.* 2015), Normalized Difference Water Index (NDWI) (Yang *et al.* 2017; Acharya *et al.* 2018), Modified Normalized Difference Water Index (MNDWI) (Sarp & Ozcelik 2016), Enhanced Water Index (EWI) (Jason & Du 2017), New Water Body Index (NWI) (Ding 2009), Shadow Water Index (SWI) (Wang *et al.* 2017), Automatic Water Extraction Index (AWEI) (Feyisa *et al.* 2014), Modified Automatic Water Extraction Index (MAWEI) (Nie *et al.* 2019), and Combined Index of NDVI and NIR for Water Body Identification (CIWI) (Li *et al.* 2015). Although these methods have shown good extraction capabilities in numerous studies, some researchers have pointed out the problem of fragmentation and discontinuity in the results extracted by these methods (Zhou *et al.* 2012).

The second type of method is the pixel-based classification method. This type of method mainly includes unsupervised classification and supervised classification (Kaplan & Avdan 2017). Unsupervised classification is a means of image classification without prior classification criteria. The main algorithms are Iterative Self Organizing Data Analysis Techniques Algorithm (ISODATA) and K-means clustering algorithm (K-Means). Supervised classification algorithms are tantamount to selecting a certain number of samples as training samples based on visual judgment and on-site investigation, and then use the decision function to classify the data in the image. The core algorithms include minimum distance method, parallelepiped method, characteristic window curve method, maximum likelihood method, etc. (Liang *et al.* 2018).

The third type of method is the object-oriented classification method. This type of method is to segment the image into objects composed of several homogeneous pixels, and these objects will be used as processing units. These processing units include not only the spectral information of the feature, but also comprehensively contain the spatial structure information, texture information, and so on (Tong *et al.* 2017). Although the object-oriented classification methods were proposed earlier and there are many related research papers (Kettig & Landgrebe 1976; Câmara *et al.* 1996), they have not served in water body extraction until recent years (He *et al.* 2016; Huang *et al.* 2016). K-nearest neighbor (KNN) pixel method (Wang *et al.* 2019), support vector machine (SVM) method (Zhang *et al.* 2019), and principal component analysis (PCA) (Duan *et al.* 2015) are the primary commonly used algorithms of this type of method. Regardless of the fact that the object-oriented classification method has been a hot topic in water research in recent years, Blaschke (2010) pointed out that the spatial resolution of satellite images was an important limiting factor for object-oriented classification techniques. This type of method had limited effect on water body extraction from remote sensing images of medium and low spatial resolution.

In addition to the above types of methods, researchers have also attempted to introduce machine learning technology to extract water bodies. Based on the OSTU algorithm, Zhao (2016) used a new water body index to complete the extraction of four main types of water body information about oceans, rivers, lakes, and reservoirs. Yu *et al.* (2017) used convolutional neural networks and logistic regression to extract water bodies. Chen *et al.* (2019) used convolutional neural network and Deeplabv3 semantic segmentation neural network to extract water bodies, respectively. The results of these studies showed that the deep learning method could effectively remove the influence of shadows and buildings.

With the optimization of algorithms, water body extraction methods are developing continuously. In order to achieve higher accuracy, improving the spatial resolution of remote sensing data and enriching image information are important ways to extract water bodies effectively. Data from satellites such as Landsat8 OLI (Hao & Wan 2019), Landsat-7 ETM+ (Xi *et al.* 2009), Sentinel (Huang *et al.* 2018), GF-1 (Deng *et al.* 2017), GF-2 (Wang *et al.* 2018), have been widely used by researchers in the extraction of water bodies. Among these satellite data, some data have low spectral spatial resolution and time resolution, some data have high spatial resolution but low time resolution, and some data have low spectral resolution. As a newly launched satellite in recent years, WFV data collected and produced by Gaofen-6 satellite (GF-6) have several advantages. Compared with the satellite data mentioned above, WFV data can realize continuous dynamic observation, with high spatial resolution (up to 16 m) and high repeated coverage (every 2 days). GF-6 WFV data contain eight bands, which are rich in band information, which provides the possibility to explore new water body methods. In addition, the width of WFV data reaches 800 km, which can realize information extraction in a larger scale. Of course, like many multispectral remote sensing data, these data are easily disturbed by the natural environment. At present, there is little research literature about data modification by the application. A few studies are mainly used in the extraction of vegetation coverage (Deng *et al.* 2021), coastal sounding mapping (Sun *et al.* 2021), rice mapping, and growth monitoring (Jiang *et al.* 2021), etc.

In this paper, first, the reflectivity of different ground objects to eight bands of GF-6WFV were extracted respectively. Through analysis, it is found that the reflectivity of the water body to the red edge band was significantly different from that of other ground objects to red edge band. Secondly, by calculating the reflectivity of different bands, it is found that different bands' operational results can produce different extraction results, and a decision tree model is constructed on the basis of constant debugging. Finally, the extraction results of our method were compared with those of traditional methods. In order to analyze the reliability of the proposed method, rivers and reservoirs in mountainous areas and scenic lakes in urban areas were both taken as research objects.

2. RESEARCH AREA AND DATA SOURCE

2.1. Study area

The study area (38°19′47″–38°44′50″N, 102°48′15″–103°19′1″E) is situated in Minqin County, Wuwei City, Gansu Province, China, with an area of about 2,100 km^2 (Figure 1). It is adjacent to the Tengger Desert in the east and the Badain Jaran Desert in the west, which belongs to a typical arid desert climate. The geographic types are mountains, plains and sand dunes, with an altitude of 1,400–2,100 m. Before the comprehensive management of the Shiyang River Basin, the total surface water in the area was less than 100 million m^3, which seriously affected people's lives and agricultural production. The geographical location of the study area is presented in Figure 1. There were two main surface water bodies with different characteristic in the study area. The first area was located near Hongya Mountain (Figure 1(d)). The water bodies in this area mainly include Shiyang River and Asia's largest desert reservoir – Hongya Mountain Reservoir. The typical ground features in this area were vegetation, farmland, highways, mountains, etc. River mudflats, mountain shadows, and vegetation shadows may affect the water body extraction effect. The second area was situated in Minqin County (Figure 1(c)). The main water bodies in this area included Qingquan Lake and the viewing lake in People's Park. The typical ground features were roads, buildings, farmland, etc. Buildings and building shadows may affect the water body extraction results.

In order to visually identify the water body more conveniently, the false color image of the remote sensing image can be obtained by combining B2, B3, and B4 in the GF-6 WFV image, as shown in Figure 2. On false color images, most water bodies appeared in a dark tone. According to the location and characteristics of the water body, the water bodies in the mountainous areas were marked and made up of four areas (Figure 2(a)). The water body of No. 1 area was Shiyang River, and the water body contains a great deal of sediment, which was light green on the false color image. The water body of No. 2 area was the tidal flat of Shiyang River, with trees interspersed with many shadows, and appears dusky black on the false color image. The water body of No. 3 area was Hongyashan Reservoir. The reservoir was deeper and the water quality was relatively clear. The false color image appeared dark blue. The water body in No. 4 area was a canal that flowed out of the Hongyashan Reservoir. The water depth was relatively shallow. Many trees grew on both sides of the canal. The false color image was also somber black. The water bodies in the urban area were mainly Qingquan Lake and the artificial lake in the People's Park, and their locations were marked as shown in Figure 2(b). The water body of No. 5 area was an artificial lake in the People's Park of Minqin County, and the water body of No. 6 area was the Qingquan Lake.

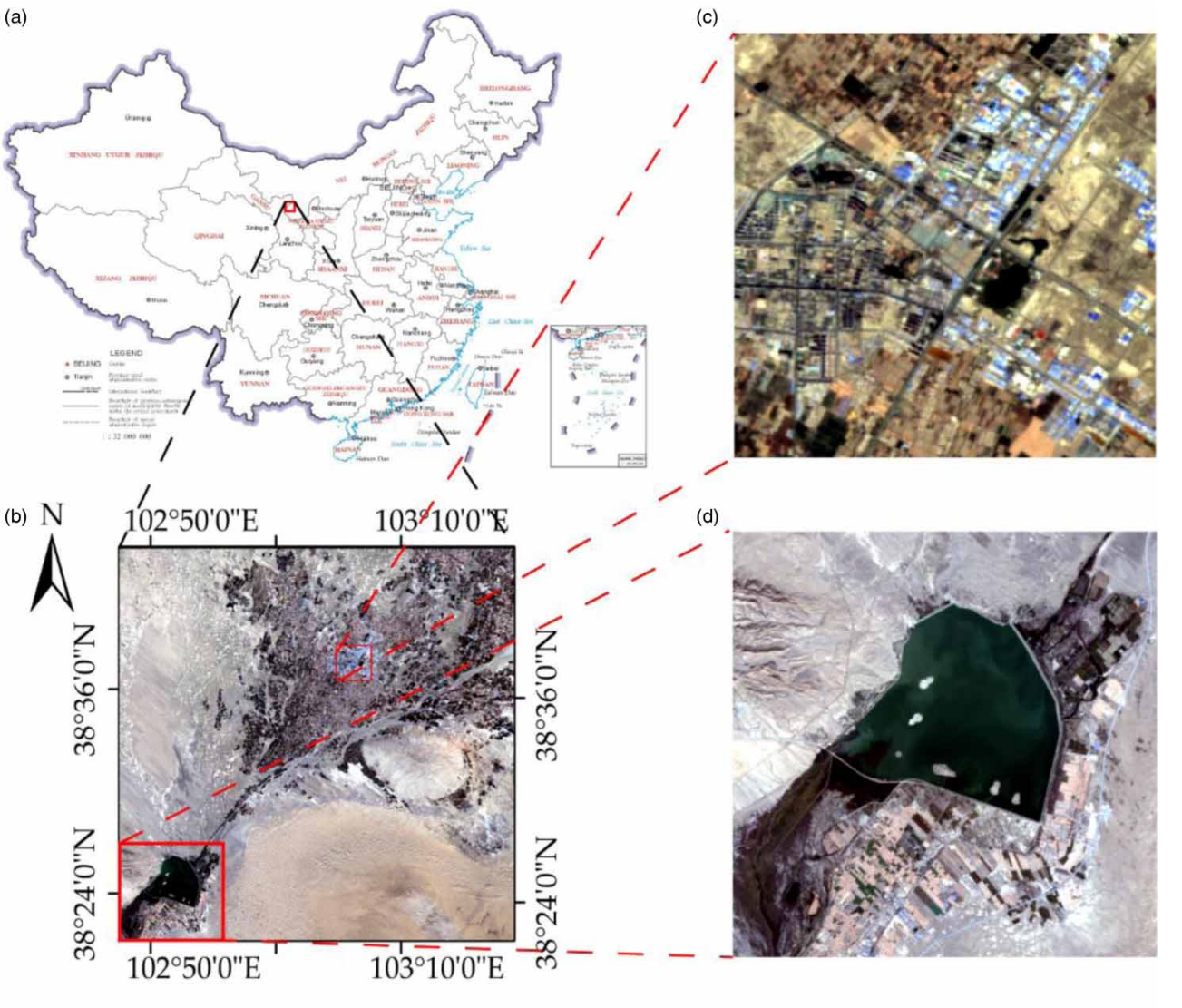

Figure 1 | The location of the study area. The red rectangle in the upper left figure (a) was the geographic location of the study area. The image on the lower left (b) was the true color image of GF-6 satellite image after preprocessing. The image on the lower right (d) was the first area. The image on the upper right figure (c) was the second area. Please refer to the online version of this paper to see this figure in colour: http://dx.doi.10.2166/nh.2021.050.

2.2. GF-6 WFV data

The Chinese GF-6 satellite was officially called into use on March 21, 2019. The satellite is equipped with a 2 meter panchromatic/8 meter multi-spectral high-resolution camera (PMS) and a 16 meter multi-spectral medium-resolution WFV camera. The observation width of PMS is 90 km, and that of WFV is 800 km. The revisit period is 2 days. The GF-6 WFV sensor covers eight frequency bands: blue, green, red, near infrared, red edge 1, red edge 2, purple, and yellow. The technical specification for GF-6 WFV data is presented in Table 1.

GF-6 WFV data used throughout this study came from the Land Survey Satellite Data Service Platform of the China Resources Satellite Application Center. The satellite image was acquired on September 29, 2019, and the weather in the study area was sunny and cloudless. Affected by atmospheric conditions, topography, and other factors, remote sensing images may cause image distortion due to assembly deformation, noise interference, and other reasons. Before conducting research on water body extraction, preprocessing such as radiation calibration, atmospheric correction, geometric correction, and image cropping must be done to reduce the adverse effects caused by factors such as the atmosphere, light, and terrain. Figure 1(b) is the true color image of GF-6 satellite image after preprocessing.

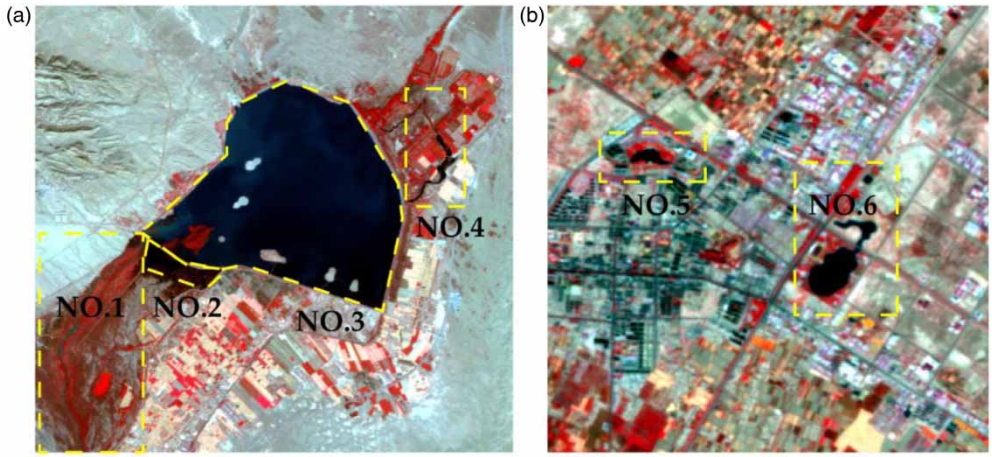

Figure 2 | False color display images of two water bodies. The image on the left (a) was false color images of the water bodies in mountainous areas. The image on the right (b) was false color images of the water bodies in urban areas.

Table 1 | Technical specification of GF-6 WFV data used in this study

Band	Channel	Central wavelength (nm)	Band width (nm)
Band 1 (B1)	Blue	485	70
Band 2 (B2)	Green	555	70
Band 3 (B3)	Red	660	60
Band 4 (B4)	Near infrared	830	120
Band 5 (B5)	Red edge 1	710	40
Band 6 (B6)	Red edge 2	750	40
Band 7 (B7)	Purple	425	50
Band 8 (B8)	Yellow	610	40

3. METHODOLOGY

GF-6 WFV data had not been applied to the study of remote sensing extraction of surface water body. Before studying the extraction method of water body, it was necessary in order to analyze the waveband emission characteristics of typical features in the study area. On the basis of field investigation and verification, the spectral features of typical feature pixels such as vegetation, lakes, rivers, farmland, roads, buildings, and shadows in the two areas of the study area were extracted. In mountainous areas, the reflectivity of pixels, mainly including vegetation, reservoir water, river water, farmland, roads, buildings, and mountain shadows were statistically analyzed. The results are presented in Figure 3. In urban areas, statistical analysis was mainly performed on the reflectance of the pixels of vegetation, lakes, farmland, buildings, and architectural shadows, as shown in Figure 4.

In Figure 3, compared with other ground features, the water body exhibited strong absorption and weak reflection characteristics for all wavebands, and the reflectivity decreased as the wavelength increases. However, the reflectivity of each waveband of the water body pixels in the Shiyang River was greater than that of the water body pixels in the Hongyashan Reservoir. The reason was that the high sediment content and turbid water quality in the Shiyang River enhanced the reflection of the wavebands. In all wavebands, the reflection differences between water bodies and non-water bodies in the two wavebands of B4 (red band) and B6 (red edge 2 band) were very significant. For the water body pixel of the reservoir, the reflectivity of the two bands B4 and B6 were significantly lower than that of other ground feature pixels. By setting reasonable thresholds in the two bands, the water body of the reservoir could be totally extracted. For the river water pixels, the reflectivity of the two bands B4 and B6 were also lower than that of other ground object pixels except the shadow pixels, but it was

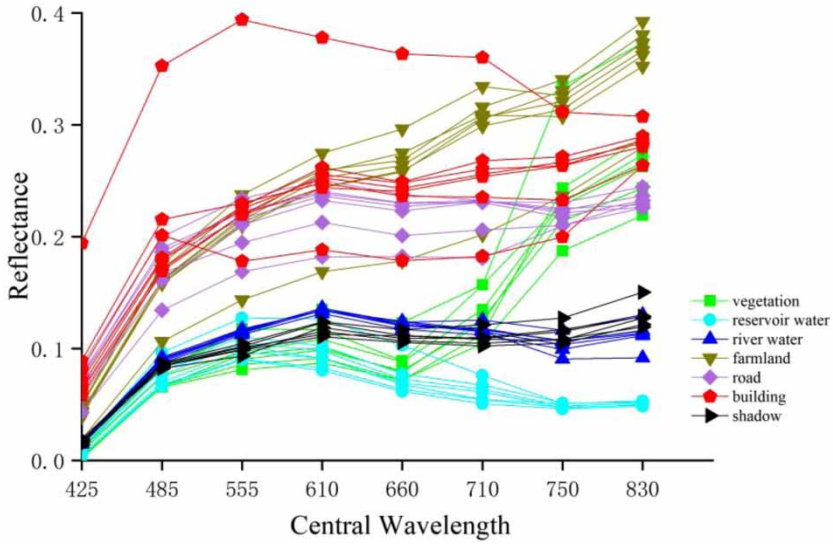

Figure 3 | Spectral curves of typical features in mountainous areas.

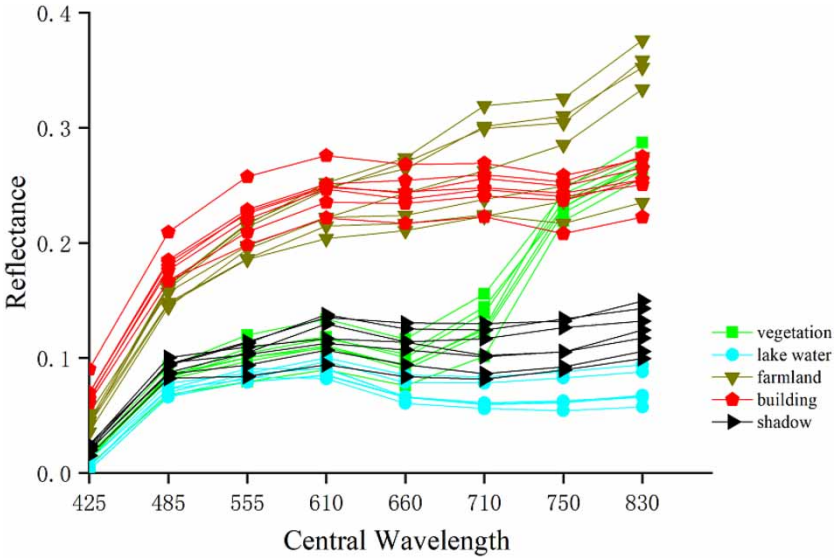

Figure 4 | Spectral curve of typical features in urban areas.

similar to the reflectivity of the shadow pixels. Therefore, when these two bands were utilized to extract pure river water pixels, the interference of shadow pixels may be greater.

In Figure 4, the reflectivity change trend of the water body pixel and non-water body pixel for the two wavebands B4 and B6 was basically similar to that in Figure 3. Different from the water pixels of the reservoir, the reflectivity of water pixels in the urban lake was very close to that of the building shadow pixels. When using the single-band threshold method, in order to extract more real water bodies pixels, the erroneous mention of shadow pixels was inevitable.

According to the above extraction results of spectral curves of separate ground objects, it can be found that the reflectivity differences of distinct bands of GF-6 WFV data to ground objects were very obvious. Abundant band information provides the possibility to explore extraction methods based on new bands, and is also beneficial to explore the application prospect of classification algorithms based on machine learning.

To validate the accuracy of the method proposed, other common methods such as single-band threshold method based on near infrared band, water index method based on NDWI, unsupervised classification method, and supervised classification

method based on SVM were mainly used to calibrate innovative methods. The research technical route of this paper is shown in Figure 5. The related methods and mechanisms is discussed in the following text.

3.1. Water body extraction based on single-band threshold method

The single-band threshold method is a classification method based on the reflection characteristics of a certain band of distinctive features in remote sensing images. The B4 band has served in numerous studies of water bodies extraction (Mondejar & Tongco 2019). But from the above analysis, it can be seen that the B6 band also could be tried to be used in water body extraction. In this study, both B4 and B6 bands were selected for the single-band threshold method. The single-band threshold method was expressed as:

$$B < T. \tag{1}$$

In Formula (1), B is the gray value of B4 or B6 band in remote sensing image. T is the gray threshold to be set.

3.2. Water body extraction based on NDWI

NDWI is a water index constructed using the green band and near infrared band. This index was considered to be able to effectively suppress vegetation and soil information, and it has also been used in surface water body extraction in many studies (Ali *et al.* 2019; Yue *et al.* 2020). The formula of NDWI was expressed as (Mondejar & Tongco 2019):

$$\mathrm{NDWI} = (\mathrm{B2} - \mathrm{B4})/(\mathrm{B2} + \mathrm{B4}) \tag{2}$$

In Formula (2), B2 is the gray value of the green light band; B4 is the gray value of the near infrared band.

The threshold of NDWI was essential for extracting water bodies. In this study, referring to the research conclusion of McFeeters (1996), 0 was used as the classification threshold. That was, pixels with NDWI values greater than 0 were considered to be water bodies, and pixels with NDWI values less than 0 were classified as non-water bodies.

3.3. Water body extraction based on decision tree of multi-band combined operation

Many scholars had noted that ground features such as shadows and buildings seriously interfere with the extraction of water bodies (Bijeesh & Narasimha 2019; Li *et al.* 2019; Li *et al.* 2020). In further analysis of the spectral reflection characteristics of the ground object pixels, the gray level results between the B2, B3, B4, and B5 bands had definite correlation with the ground object pixels. By subtracting the gray values of the B2 and B4 bands, the difference of most water pixels was greater

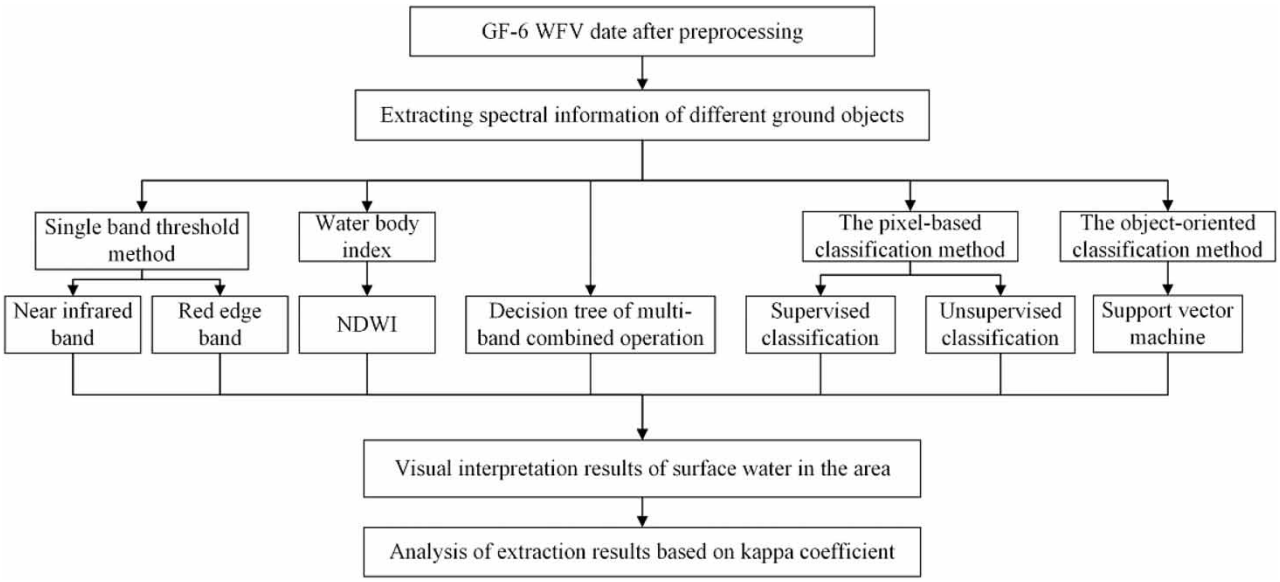

Figure 5 | Technical route of surface water body extraction based on various methods.

than 0, and the difference of other non-water feature pixels was mostly less than 0. The difference of a few road pixels was greater than 0, and the difference of most shadow pixels was less than −110. By subtracting the gray values of the B5 and B3 bands, the difference between most water pixels and shadow pixels was less than 50, and the difference between extra feature pixels was mostly greater than 0. Combined with the debugging results in the single-band threshold method, when the gray value of the B6 band was less than 1,100, the removal of non-aqueous features such as buildings and roads could be achieved. Therefore, the non-water pixels could be removed step by step by making effective use of the reflection characteristics of different bands for the combined operation. In the study, a decision tree model was constructed built on the above-mentioned discovered rules, which removed the interference of shadows and vegetation pixels, then removed the interference of road pixels and building pixels, and finally leaves the surface water pixels. The decision tree model is presented in Figure 6.

3.4. Water body based on supervised classification and unsupervised classification

In the study, both unsupervised classification and supervised classification were used for water body extraction in two areas.

The two main algorithms ISODATA and K-means were both used for unsupervised separation. Unsupervised classification was based on the pixel characteristics of satellite images. The number of classification types had a definite impact on the classification results. In the study, 15 types of features were set for unsupervised classification. After the classification results were obtained, through the visual interpretation, the pixels in the classified image were sorted into two categories: water and non-water.

When using supervised classification, it was necessary to select appropriate training samples. The types of ground features in the study area were complex. If the training sample type was not properly selected, some features with complex pixel features may be ignored, which would affect the extraction effect. The strategy included in this study was to simplify the sample types. In mountainous areas, the water bodies of reservoirs, rivers, canals, and floodplains were regarded as one type of sample type, and vegetation, buildings, farmland, roads, shadows, and other features were collectively classified as another type of sample type. In urban areas, the water bodies of Qingquan Lake and artificial lakes were considered as one type of sample type, and buildings, roads, vegetation, shadows, and other features were collectively classified as another type of sample type. When sampling, for water bodies, there must be typical pixels selected as samples in the six regions in Figure 2.

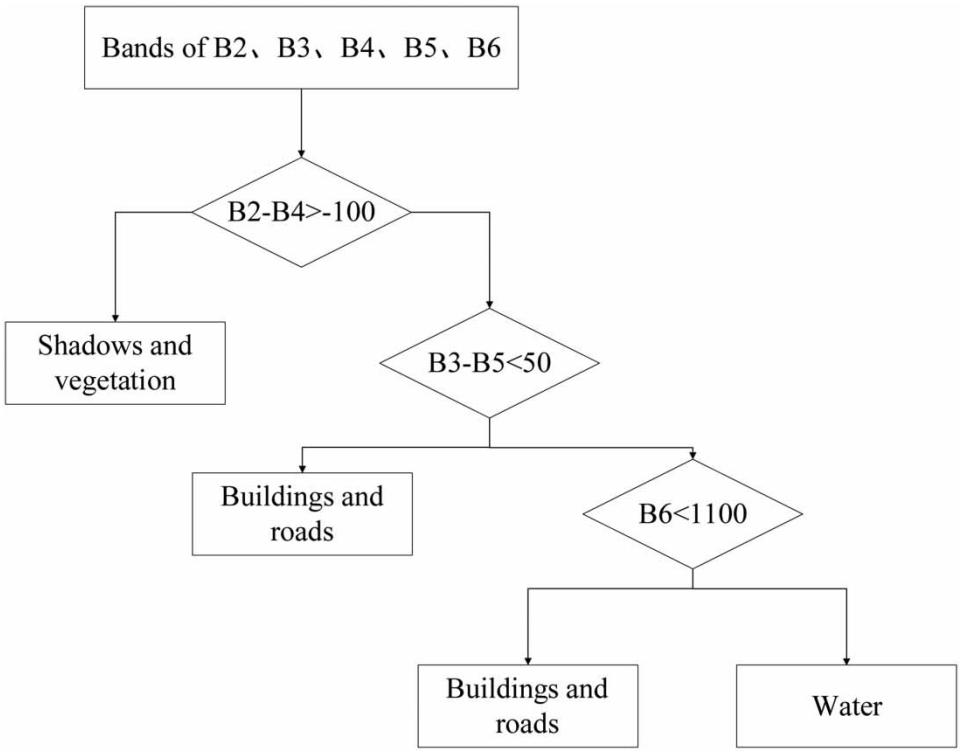

Figure 6 | Decision tree model based on multi-band combined operation.

For non-aqueous bodies, the sample sampling volume should be increased, and the various non-aqueous features on the image should be covered as much as possible. Among several algorithms for supervised classification, the support vector machine (SVM) algorithm is essentially a binary classification algorithm that fundamentally works to separate data points into two classes, and it is more suitable for solving the problems such as few samples, nonlinearity, and local minima (Zhang *et al.* 2019). Thus, the SVM algorithm was selected as the supervised classification method in this study.

3.5. Accuracy evaluation

In the study, the real water boundary in most areas was established by field survey. By plotting the measured water boundary on the remote sensing image, the actual water pixel can be interpreted intuitively on the satellite image. Because the spatial resolution of GF-6 WFV data is 16 meters, some pixels will contain many different types of ground objects such as water, land, and vegetation. For these pixels, in visual interpretation, if the area of non-water features in the pixel exceeds 1/2, the pixel is regarded as non-water. In the study, some areas were not in a position for the boundary of a water body to be measured. In these few areas, the real water pixels are determined in GF-6 WFV images by comparing with the visually interpreted water pixels in GF-2 PMS images with higher spatial resolution obtained in the same period. The total number of pixels in the mountain image was 548,340, and the total number of real water body pixels was 89,271. The total number of pixels in the urban image was 96,408, and the total number of real water pixels was 878.

At present, there is no uniform standard for the comparison of water body extraction accuracy. Some studies have pointed out that the construction of confusion matrix to calculate the overall classification accuracy, Kappa coefficient, overall accuracy, misclassification error, missing error, and so on are often used by remote sensing processing software (Wang & Qin 2018), which are also used to compare the accuracy of water extraction methods (Du *et al.* 2014; Sekertekin 2021).

Kappa coefficient was utilized to test the consistency of the classification effect. The calculation of Kappa coefficient is based on a confusion matrix. In the study, the water body extraction results obtained by different methods and the classification results of visual interpretation were utilized to construct the confusion matrix and calculate the corresponding Kappa coefficient. In order to better analyze the differences between the extraction methods, the overall accuracy, the omission error, and the misclassification error of each extraction result were also calculated. Overall accuracy is the percentage of all correctly identified pixels in remote sensing images. Omission error is the probability that a real water body pixel is incorrectly classified into other categories, and the misclassification error is the probability that a non-water body pixel is incorrectly classified as a water body. The extraction of water body in the study was a two-class problem, so only a two-order confusion matrix was required to be constructed. Kappa calculation formula is as follows:

$$kappa = \frac{p_0 - p_e}{1 - p_0} \tag{3}$$

$$p_0 = \frac{\sum_{i=1}^{n} a_{ii}}{N} \tag{4}$$

$$p_e = \frac{\left(\sum_{j=1}^{n} a_{1j} \times \sum_{i=1}^{n} a_{i1} + \sum_{j=1}^{n} a_{2j} \times \sum_{i=1}^{n} a_{21}\right)}{N \times N} \tag{5}$$

In the above formula, N is the total number of pixels in the study area. The n is the order of the confusion matrix, and the value in the study is 2; a_{ij} is the constituent element of the confusion matrix.

4. RESULTS AND DISCUSSION

4.1. Extraction of water bodies in mountainous areas

Extraction results of water bodies in mountainous areas based on different methods are illustrated in Figure 7, where the water body pixels are marked in blue. Figure 7(a) is the real water body result of visual interpretation. Figure 7(b) and 7(c) are the water body extraction results based on the single-band threshold method of B4 and B6, respectively. The water body extraction results of the two bands were relatively similar, but the extraction of water pixels based on the B6 band was greater than the extraction results based on the B4 band. The Shiyang River in No. 1 area was a continuous river, but the pixels in the extraction results were broken, and only some real water pixels were extracted. Extraction results of the

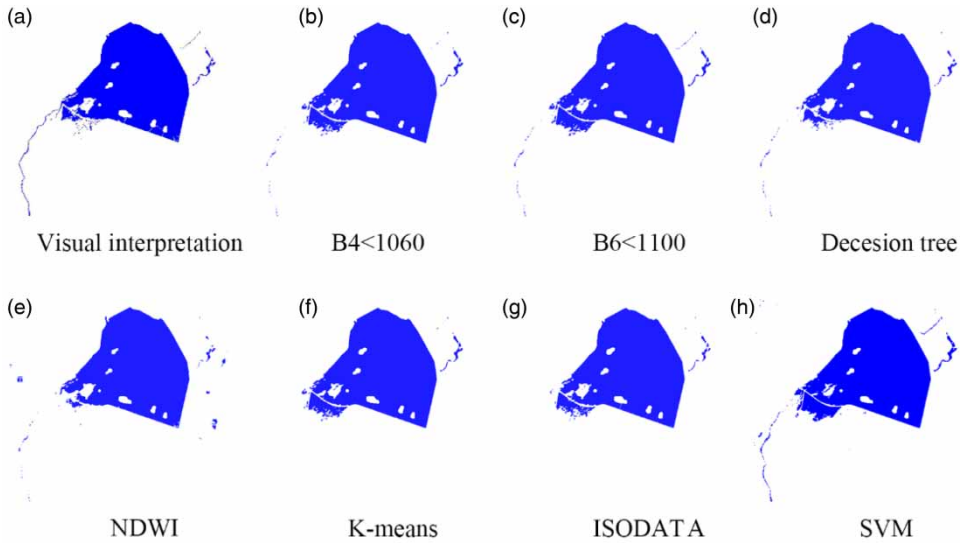

Figure 7 | Extraction results of water bodies in mountainous areas based on different methods. Please refer to the online version of this paper to see this figure in colour: http://dx.doi.10.2166/nh.2021.050.

single-band threshold method based on the B6 band were slightly better than those based on the B4 band. The water bodies of No. 2 and No. 3 areas had been over-extracted, and a large number of non-water body pixels were incorrectly classified as water bodies. The feature types of the pixels extracted by mistake were mainly vegetation and shadows on the floodplain in No. 2 area and aquatic plants in No. 3 area. The spectral information of pixels in these places was complicated, especially the presence of shadows seriously interferes with the extraction results. Finally, the threshold method based on the B4 band had a limited effect on the extraction of the small water channel in the upper right corner of the water body in No. 4 area, and the threshold method based on the B6 band had a better effect. Figure 7(d) is the extraction result obtained by the decision tree method based on multi-band combination operation. Compared with the results in Figure 7(b) and 7(c), the water body pixels of Shiyang River extracted from No. 1 area in Figure 7(d) were almost the same as the results in Figure 7(c). The water pixels extracted in area No. 2 were significantly less than the results in Figure 7(b) and 7(d). By comparing with real water body pixels visually interpreted in Figure 7(a), this method was more effectively avoiding the interference of vegetation and shadows in the floodplain. However, when extracting small water bodies in No. 4 area, the extraction effect of this method was not as good as the single-band threshold method. Figure 7(e) shows the extracted results based on the NDWI. Only the water body extraction result in No. 3 area was closer to the result of visual interpretation, and many real water body pixels in the other three areas were omitted. At the same time, many pixels of buildings and roads in the extraction results were incorrectly classified as water bodies. Figure 7(f) is the extraction result of unsupervised classification based on K-means algorithm, and Figure 7(g) is the extraction result of unsupervised classification based on ISODATA algorithm. Regardless of whether the ISODATA or K-means algorithm was used, the water pixels of the Shiyang River in the No. 1 area had not been effectively extracted. Based on these two algorithms, the water body extraction results in the other three regions were very similar. The reason why the Shiyang River in No. 1 area was not effectively extracted may be that the sediment content in the river water was higher, causing the pixels to be more akin to the soil. From the extracted results, it can be concluded that the unsupervised classification method was not applicable to areas where the spectral information of pixels was significantly altered due to the difference in water quality.

Figure 7(h) is the extraction result of the supervised classification method based on the SVM algorithm. This method was quite effective for the extraction of real water pixels in all four areas. Especially, the water body extraction results in No. 1 and No. 4 areas were closer to the results of visual interpretation. However, it is worth noting that this method incorrectly classifies many non-water pixels in the four areas as water pixels. The reason for this situation may be that the water quality and pixel characteristics in the four areas were changed, and there may be deviations in the selection of training samples in the study. This exposed the problems of supervised classification in water body extraction: classification required extraordinary purity of training samples, and training samples should be typical and representative. When choosing this method, a priori knowledge of the research field was required, so it was difficult to achieve automatic extraction of water bodies.

4.2. Extraction of water bodies in urban areas

Extraction results of water bodies in urban areas based on different methods are shown in Figure 7, where the water body pixels are also marked in blue. Figure 7(a) is the real water body result of visual interpretation.

There were fewer types of ground features in urban areas than in mountainous areas, and there were fewer interference factors in the extraction process. The types of municipal water bodies were single, and the spectral curves of the water body pixels in areas of No. 5 and No. 6 were almost the same. The water quality of the two water bodies in the No. 5 area and the No. 6 area were both very good, and the boundaries of the water bodies were clearer.

In Figure 8, the water body extraction result obtained by the decision tree method based on multi-band combined operation (Figure 8(d)) was better than other methods. This method effectively extracted real water pixels, and avoided erroneous extraction of non-water pixels. In the extraction results of the supervised classification method based on SVM algorithm, although there were not many pixels extracted by mistake, the pixels of real water bodies were obviously omitted.

Among the results obtained by other methods, compared with the results of visual interpretation, the single-band threshold method (Figure 8(b) and 8(c)) and the unsupervised classification method (Figure 8(f) and 8(g)) had similar effects in extracting real water pixels. However, in these four results, there are more non-water pixels extracted by mistake than in Figure 8(d), especially, the large number of shadow pixels of buildings in Figure 8(f) and 8(g) were incorrectly classified as water bodies. In the extraction results based on the NDWI, many real water pixels in areas of No. 5 and No. 6 were omitted, and a large number of non-water pixels were also incorrectly extracted. The difference from the aforementioned four consequences was that the mis-mentioned pixel types in Figure 8(e) were mainly buildings and a small amount of building shadows. At this time, the NDWI index method could better remove the interference of the building shadow, but it could not avoid the influence of the building itself.

4.3. Accuracy analysis of different methods

Water body extraction results obtained based on different methods were compared and analyzed with the real water body manually interpreted, and confusion matrices were constructed respectively. Kappa coefficient, overall accuracy, misclassification error, and omission error could be calculated separately. The results are shown in Tables 2 and 3.

Table 2 shows the accuracy results of different methods for water body extraction in mountainous areas. The Kappa coefficient of the decision tree method based on multi-band combination was the highest, reaching 97.73%, and the Kappa coefficient of the supervised classification method based on SVM was the lowest, being 94.47%. Omission error values and misclassification error values of the decision tree based on multi-band combination operation were relatively low. Both were 1.89%. This method not only realized the effective extraction of water body pixels but also effectively avoided the wrong extraction of non-water body pixels. Although the omission error of water body extraction based on SVM was

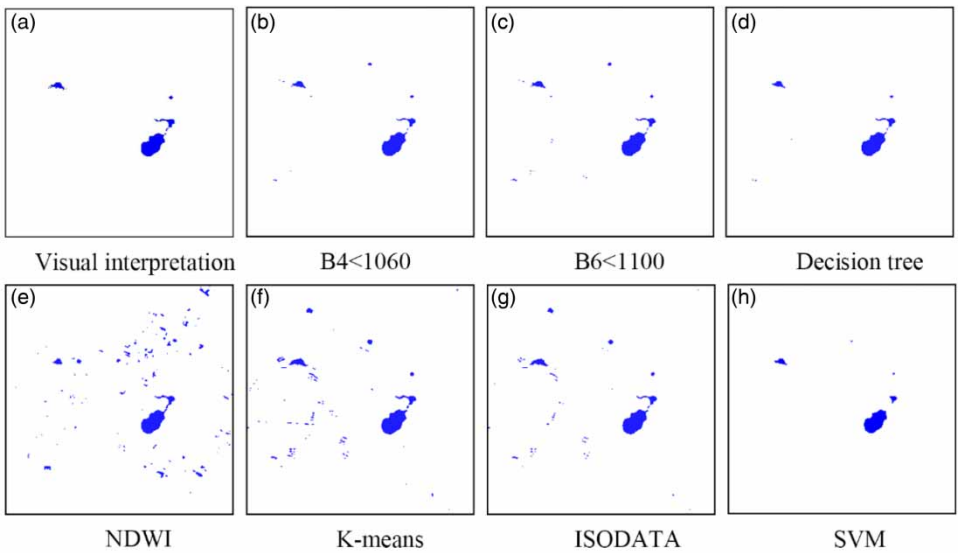

Figure 8 | Extraction results of water bodies in urban areas based on different methods.

Table 2 | The accuracy of different methods for water body extraction in mountainous areas

Serial number	Method	Kappa (%)	Overall accuracy (%)	Misclassification error (%)	Omission error (%)
1	Single-band threshold method based on B4 band	96.35	98.99	4.49	1.55
2	Single-band threshold method based on B6 band	96.18	98.95	5.01	1.26
3	Water index method based on NDWI	96.8	99.12	2.6	2.75
4	Unsupervised classification method based on ISODATA algorithm	96.61	99.07	2.88	2.79
5	Unsupervised classification method based on K-means algorithm	96.16	98.94	4.22	2.15
6	Supervised classification based on SVM	94.97	98.59	7.3	0.8
7	Decision tree model method based on multi-band combined operation	97.73	99.38	1.89	1.89

Table 3 | The accuracy of different methods for water body extraction in urban areas

Serial number	Method	Kappa (%)	Overall accuracy (%)	Misclassification error (%)	Omission error (%)
1	Single-band threshold method based on B4 band	94.06	99.89	6.51	5.23
2	Single-band threshold method based on B6 band	93.21	99.87	8.99	4.32
3	Water index method based on NDWI	65.66	99.14	48.29	8.54
4	Unsupervised classification method based on ISODATA algorithm	84.24	99.66	26.25	1.36
5	Unsupervised classification method based on K-means algorithm	76.79	99.46	37.1	0.56
6	Supervised classification based on SVM	91.63	99.85	1.31	14.35
7	Decision tree model method based on multi-band combined operation	94.41	99.90	4.42	6.6

the smallest of all methods, the error of misclassification was the highest. In the study, the training samples of the water pixels were carefully selected, but due to the complex water types in the mountainous areas, the extraction results were still not ideal.

In addition to the above two methods, Kappa coefficients of the extraction results obtained by other methods were about 96%, but there were differences in the error of misclassification and omission. The single-band threshold method based on the B4 band and the B6 band had a relatively low missed scoring error and a higher missed scoring. The single-band threshold method could better extract the real water pixels in the four regions, but many non-water pixels were mistakenly classified as water pixels, which was consistent with the result in Figure 7. Both extraction results based on NDWI and the unsupervised classification method had high error values for misclassification and omission. The disadvantages of the unsupervised classification method tended to be unable to effectively extract the water in the No. 1 area. The water body index law based on NDWI tends to extract non-water body pixels incorrectly.

Table 3 shows the accuracy results of different methods for water body extraction in urban areas. The Kappa coefficient of the decision tree method based on multi-band combination operation was the highest, reaching 94.41%, and the K-means algorithm-based unsupervised classification had the lowest Kappa coefficient of 76.79%. Kappa coefficients of the single-band threshold method extraction results based on B4 and B6 also reached 94.06% and 93.21%, respectively. The single-band threshold method had a better effect on water body extraction in urban areas, and the single-band threshold method based on the B6 band found and proposed in this study also showed very good classification performance. Both the unsupervised classification method and NDWI had relatively high misclassification errors in the extraction results, which were in

accordance with the analysis results in Figure 8. It is worth noting that among all the methods, the omission error in the extraction results based on SVM was very high, reaching 14.35%. The reason may be that the water pixels at the boundary of the lake were not included in the training samples, and the pixel information of these pixels may be different from the pure water pixels in the center of the lake.

From the above analysis results, the decision tree method based on the combined operation of B2, B3, B4, B5, and B6 in this study has achieved very good results in surface water extraction in mountainous and urban areas.

4.4 Application value of red edge band

Improving the accuracy of remote sensing extraction of surface water is part of the core objectives of a large number of studies. In recent years, in order to improve the accuracy, researchers have put forward many new water indexes, such as MOWI (modified optimization water index) (Moradi *et al.* 2017), Terrain indices (MrVBF and HAND) (Huang *et al.* 2017), Sum 457 (sum of near infrared and two shortwave infrared bands) (Zeng *et al.* 2017), and so on. With the increasing popularity of machine learning algorithms, a large number of related methods based on machine learning have been applied to water remote sensing extraction, and some new classification algorithms have emerged (Isikdogan *et al.* 2017; Li *et al.* 2017). In addition, methods based on spectral mixture analysis are becoming ever more popular, because they can estimate the proportion of various spectra existing in pixels, which can better classify pixels (Bijeesh & Narasimhamurthy 2020). However, no matter which extraction method, it is inseparable from the spectral characteristics of remote sensing data. Therefore, it continues to be of great significance to explore the water extraction ability of different characteristic spectra, provided that remote sensing data containing more spectra can be obtained. The above research of Sections 4.1–4.3 showed that the red edge band itself has similar surface water extraction ability to the near infrared band. Whether in mountainous areas or urban areas, the single-band threshold method based on red edge 2 bands in GF-6 WFV data was similar to the single-band extraction accuracy based on near infrared bands, both of which were above 93%. The multi-band combination decision tree method proposed in this study was obtained through a great deal of constant debugging, and its extraction ability was the best among the methods adopted in this study. Compared with several typical conventional remote sensing extraction methods of surface water, the two newly discovered extraction methods using red sideband would not cause significant differences in extraction effects due to altered water environment. In sharp contrast, the extraction effect of NDWI was more easily affected by the environment of water. Kappa value of the index reached 96.8% in mountainous areas, but only 65.66% in cities.

Although the red edge band showed unforgettable extraction ability in this study, it still failed to achieve complete and correct extraction of the water body. The existence of shadows will still cause interference. Therefore, water extraction methods related to the red edge band and the water extraction methods based on GF-6 WFV data are still worth improving.

5. CONCLUSIONS

In this paper, the GF-6 WFV data were taken as the remote sensing data source, and the water bodies located in Hong Yashan mountainous area and county town in Minqin, Gansu Province were taken as the extraction objects, and the remote sensing extraction method was studied. The research further expands the application prospect of red edge band in the remote sensing field. Research results fully demonstrate that the red edge waveband extraction method we found and proposed had high utilization value in water extraction. The research drew the following conclusions.

Among the extraction methods based on different mechanisms employed in this research, the decision tree method based on multi-band combined operation obtained the best extraction results in both regions. Kappa coefficient of extraction result of water bodies in mountainous areas was 97.73%. Both the error of omission and the error of misclassification were 1.89%. Kappa coefficient of extraction consequence of water bodies in urban areas was 94.41%. The missing scoring error was 4.42%, and the misclassification error was 6.6%. The decision tree model used two red edge bands in the GF-6 WFV data, and successfully solved the problem of incorrect mention of shadows, vegetation, and buildings. It was necessary to extract and analyze the spectral information of the ground object pixels in advance in the process of building the model, so as to set specific thresholds for each layer. However, this decision tree model could obtain high-precision water body results in both mountainous and urban areas. The research results fully showed that this method could serve as a new method for water body extraction. In addition, the single-band threshold method based on the B6 band also achieved excellent water body extraction results in both mountainous and urban areas. The single-band threshold method based on the B6 band had a Kappa coefficient of 96.18% in mountain water bodies, and a Kappa coefficient of 93.21% in urban water bodies.

In order to be compared with the proposed method, four conventional methods were utilized to extract water from the study area by remote sensing. The pixel-based classification method used in the study had poor water extraction results. Regardless of the fact that Kappa coefficients of the two algorithms of the unsupervised classification method in mountain water body extraction results reached more than 96%, it was virtually impossible to achieve effective extraction of the water body pixels of the Shiyang River. The water body extraction results of these two algorithms in urban areas were even lower than 85%. Kappa coefficients of the water body extraction results obtained by using the supervised classification method of the SVM algorithm in the two areas were greater than 91%, but this method relied too much on the purity of the training samples. In areas with complex water features, the reliability of the method may become unstable. However, in the case that water information needs to be extracted quickly and the extraction accuracy is low, the supervised classification method still has good application value. NDWI showed good results in mountain water extraction, but it was very bad in urban water extraction, and the interference of buildings was very serious.

In this study, due to various reasons, it is impossible to measure more water bodies in different areas, which led to the study area being restricted to Minqin, China. In checking to ensure the reliability of the proposed method, water bodies located in mountainous areas and water bodies located in urban areas were selected as two independent research objects. In order to further verify the reliability of the water body method based on the red sideband, it is necessary to study more water bodies located in different regions in the future. At the same time, the application of the red sideband in remote sensing extraction of water resources needs further development, such as developing a general water resources index based on red sideband.

ACKNOWLEDGEMENTS

The authors deeply appreciate the anonymous reviewers and the editor's constructive comments and suggestions, all of which have led to great improvements in the presentation of this article.

AUTHOR CONTRIBUTIONS

Conceptualization, D.W. and Z.L.; Methodology, Z.L.; Software, Z.L.; Validation, Z.D. (Zhengdong Deng) and Z.D. (Zhibin Ding); Formal analysis, H.Z. and H.N.; Investigation, G.W. and H.X.; Data curation, H.Z. and X.Z.; Writing – original draft preparation, Z.L.; Writing – review and editing, Y.S. and J.Z.; Project administration, D.W. All authors have read and agreed to the published version of the manuscript.

CONFLICTS OF INTEREST

The authors declare no conflict of interest.

FUNDING

This research received no external funding.

DATA AVAILABILITY STATEMENT

All relevant data are included in the paper or its Supplementary Information.

REFERENCES

Acharya, T. D., Subedi, A. & Lee, D. H. 2018 Evaluation of water indices for surface water extraction in a Landsat 8 scene of Nepal. *Sensors* **18**, 2580.

Ali, M., Dirawan, G., Hasim, A. & Abidin, M. 2019 Detection of changes in surface water bodies urban area with NDWI and MNDWI methods. *Int. J. Adv. Sci. Eng. Inf. Technol.* **9**, 946–951.

Bijeesh, T. V. & Narasimha, M. 2019 A comparative study of spectral indices for surface water delineation using Landsat 8 Images. *2019 International Conference on Data Science and Communication (IconDSC)*, IEEE, Bangalore, India.

Bijeesh, T. V. & Narasimhamurthy, K. N. 2020 Surface water detection and delineation using remote sensing images: a review of methods and algorithms. *Sustain. Water Resour. Manag.* **6**, 68.

Blaschke, T. 2010 Object based image analysis for remote sensing. *ISPRS J. Photogramm. Remote Sens.* **65**, 2–16.

Câmara, G., Souza, R., Freitas, U. & Garrido, J. 1996 Integrating remote sensing and GIS by object-oriented data modelling. *Comput. Graphics* **20**, 395–403.

Chen, Q., Zheng, L., Li, X., Xu, C., Wu, Y., Xie, D. & Liu, L. 2019 Water body extraction from high-resolution satellite remote sensing image based on deep learning. *Geogr. Geo-Inf. Sci.* **35**, 43–49.

Deng, F., Zhang, X., Hua, L. & Li, Z. 2017 A surface water body extraction method based on domestic remote sensing imagery of high resolution. *Hydrogeol. Eng. Geol.* **44**, 43–50.

Deng, Z. D., Lu, Z., Wang, G. Y., Wang, D. Q., Ding, Z. B., Zhao, H. F., Xu, H. L., Shi, Y., Cheng, Z. J. & Zhao, X. N. 2021 Extraction of fractional vegetation cover in arid desert area based on Chinese GF-6 satellite. *Open Geosci.* **13**, 416–430.

Ding, F. 2009 Study on information extraction of water body with a new water index (NWI). *Sci. Surv. Mapp.* **34**, 155–157.

Du, Z. Q., Li, W. B., Zhou, D. B., Tian, L. Q., Ling, F. & Wang, H. L. 2014 Analysis of Landsat-8 OLI imagery for land surface water mapping. *Remote Sens. Lett.* **5**, 672–681.

Duan, Q., Meng, L., Fan, Z., Hu, W. & Xie, W. 2015 Applicability of the water information extraction method based on GF-1 image. *Remote Sens. Land Resour.* **27**, 79–84.

Feyisa, G., Meilby, H., Fensholt, R. & Proud, S. 2014 Automated water extraction index: a new technique for surface water map-ping using Landsat imagery. *Remote Sens. Environ.* **140**, 23–35.

Gong, W., Wang, P., Wang, S., Zhou, Y. & Cao, K. 2018 Methods of water body extraction in boundary river based onGF-2 satellite remote sensing image of high resolution. *J. Eng. Heilongjiang Univ.* **9**, 1–7.

Hao, Y. & Wan, L. 2019 Comparative analysis of water information extraction methods in Harbin area based on landsat8 OLI images. *Nat. Sci. J. Harbin Norm. Univ.* **35**, 87–92.

He, Y., Zhang, X. & Hua, L. 2016 Object-based distinction between building shadow and water in high-resolution imagery using fuzzy-rule classification and artificial bee colony optimization. *J. Sens.* 2385039. https://doi.org/10.1155/2016/2385039.

Huang, S., Ding, J. & Li, Y. 2016 Study of water information extraction based on domestic GF-1 remote sensing image by using object-oriented method. *Yangtze River* **47**, 23–28.

Huang, C., Nguyen, B. D., Zhang, S. Q., Cao, S. M. & Wagner, W. 2017 A comparison of terrain indices toward their ability in assisting surface water mapping from Sentinel-1 data. *ISPRS Int. J. Geo-Inf.* **6**, 140.

Huang, W., DeVries, B., Huang, C., Lang, M., Jones, J., Creed, I. & Carroll, M. 2018 Automated extraction of surface water extent from Sentinel-1 data. *Remote Sens.* **10**, 797.

Isikdogan, F., Bovik, A. C. & Passalacqua, P. 2017 Surface water mapping by deep learning. *IEEE J. Sel. Top. Appl. Earth Obs. Remote Sens.* **10**, 4909–4918.

Jason, Y. & Du, X. 2017 An enhanced water index in extracting water bodies from Landsat TM imagery. *ANN GIS* **23** (3), 141–148.

Jiang, X., Fang, S., Huang, X., Liu, Y. & Guo, L. 2021 Rice mapping and growth monitoring based on time series GF-6 images and red-edge bands. *Remote Sens.* **13**, 579.

Kaplan, G. & Avdan, U. 2017 Object-based water body extraction model using Sentinel-2 satellite imagery. *Eur. J. Remote Sens.* **50**, 137–143.

Kasvi, E., Salmela, J., Lotsari, E., Kumpula, T. & Lane, S. 2019 Comparison of remote sensing-based approaches for mapping bathymetry of shallow, clear water rivers. *Geomorphology* **333**, 180–197.

Kettig, R. & Landgrebe, D. 1976 Classification of multispectral image data by extraction and classification ofhomogeneous objects. *IEEE Trans. Geosci. Electron.* **14**, 19–26.

Li, H., Wang, X., Dai, S. & Tian, G. 2015 Flood monitoring in Hainan Island based on HJ-CCD data. *Trans. CSAE* **31** (17), 191–198.

Li, N., Martin, A. & Estival, R. 2017 An automatic water detection approach based on Dempster–Shafer theory for multi-spectral images. In: *2017 20th International Conference on Information Fusion*, Xi'an, China.

Li, L., Yan, Z., Shen, Q., Cheng, G., Gao, L. & Zhang, B. 2019 Water body extraction from very high spatial resolution remote sensing data based on fully convolutional networks. *Remote Sens.* **11**, 1162–1181.

Li, D., Wu, B., Chen, B., Qin, C., Wang, Y., Zhang, Y. & Xue, Y. 2020 Open-surface river extraction based on Sentinel-2 MSI imagery and DEM data: case study of the Upper Yellow River. *Remote Sens.* **12**, 2737.

Liang, S., Wang, Q., Zhang, C., Zhang, M., Sun, H. & Ren, H. 2018 Extraction method of high dive site mining area water-body based on GF-2 data. *Mine. Surv.* **46**, 5–9.

Liu, S., Wang, M., Yang, S., Yang, M. & Yang, L. 2019 Extraction accuracy and stability analysis of different waterbody index models in GF-2 images. *Bull. Surv. Mapp.* **8**, 135–139.

McFeeters, S. 1996 The use of the normalized difference water index (NDWI) in the delineation of open water features. *Int. J. Remote Sens.* **17**, 1425–1432.

Mondejar, J. & Tongco, A. 2019 Near infrared band of Landsat 8 as water index: a case study around Cordova and Lapu-Lapu City, Cebu, Philippines. *Sustain. Environ. Res.* **29**, 16.

Moradi, M., Sahebi, M. & Shokri, M. 2017 Modified optimization water index (MOWI) for Landsat-8 Oli/Tirs. *ISPRS-Int. Arch. Photogramm. Remote Sens. Spatial Inf. Sci.* **XLII**, 185–190.

Nie, Y., Yu, M. & Lan, T. 2019 Research on water information extraction based on MAWEI index. *J. Earth Environ.* **10**, 281–290.

Pierpaolo, S. 2018 Water for agriculture, irrigation management. *Appl. Soil Ecol.* **123**, 793–796.

Sarp, G. & Ozcelik, M. 2016 Water body extraction and change detection using time series: a case study of Lake Burdur, Turkey. *J. Taibah Univ. Sci.* **11** (3), 381–391.

Sekertekin, A. 2021 A survey on global thresholding methods for mapping open water body using Sentinel-2 satellite imagery and normalized difference water index. *Arch. Computat. Meth. Eng.* **28**, 1335–1347.

Sun, M. X., Yu, L. J., Zhang, P., Sun, Q. Q., Jiao, X., Sun, D. F. & Liu, F. 2021 Coastal water bathymetry for critical zone management using regression tree models from Gaofen-6 imagery. *Ocean Coast. Manage.* **204**, 105522.

Tong, L., Yan, Q., Luo, C. & Du, Y. 2017 Water body information extraction based on NDWI segmentation and object-oriented method. *Geo. Spat. Inf.* **15**, 57–59.

Wang, J., Ding, J., Zhang, C. & Chen, W. 2017 Method of water information extraction by improved SWI based on GF-1 satellite image. *Remote Sens. Land Resour.* **29**, 29–35.

Wang, H. & Qin, F. 2018 Summary of the research on water body extraction and application from remote sensing image. *Sci. Surv. Mapp.* **43** (5), 23–32.

Wang, J., Nuan, R., Chai, Y. & Lin, P. 2018 Object-oriented urban water information extraction based on GF-2. *Geo. Spa. Inf.* **16**, 34–37. + 40.

Wang, X., Xu, M., Li, K. & Ning, C. 2019 Effective water body extraction method for high resolution remote sensing images. *Comput. Eng. Appl.* **55**, 145–151 + 207.

Wu, X., Zheng, Y., Wu, B., Tian, Y., Han, F. & Zheng, C. 2016 Optimizing conjunctive use of surface water and groundwater for irrigation to address human-nature water conflicts: a surrogate modeling approach. *Agric. Water Manage.* **163**, 380–392.

Xi, X., Shen, N. & Li, X. 2009 Research of automatic extraction of water bodies on ETM+ images. *Comput. Eng. Des.* **30**, 993–996.

Xu, R., Zhang, Z. & Zhao, C. 2015 Different models used in extraction of lake water body based on MODIS date. *Remote Sens. Inf.* **30**, 111–118.

Yang, X., Zhao, S., Qin, X., Zhao, N. & Liang, L. 2017 Mapping of urban surface water bodies from sentinel-2 MSI imagery at 10 m resolution via NDWI-based image sharpening. *Remote Sens.* **9**, 596.

Yu, L., Wang, Z., Tian, S., Ye, F., Ding, J. & Kong, J. 2017 Convolutional neural networks for water body extraction from landsat imagery. *Int. J. Comput. Intell. Appl.* **16**, 1750001.

Yue, H., Li, Y., Qian, J. & Liu, Y. 2020 A new accuracy evaluation method for water body extraction. *Int. J. Remote Sens.* **41**, 1–32.

Zeng, L. F., Schimtt, M., Li, L. & Zhu, X. X. 2017 Analysing changes of the poyang lake water area using sentinel-1 synthetic. *Int. J. Remote Sens.* **38**, 7041–7069.

Zhang, M. 2008 Extracting water body information with improved model of spectral relationship in a higher montain area. *Geogr. Geo-Inf. Sci.* **24**, 14–16.

Zhang, D., Yang, S., Wang, Y. & Zheng, W. 2019 Refined water body information extraction of three gorges reservoir by using GF-1 satellite data. *Yangtze River* **50**, 233–239.

Zhao, Z. 2016 A new water index extracting water information automatically from landsat based on OSTU. *Geomatics Spat. Inf. Technol.* **39**, 57–60.

Zhao, X., Wang, P., Chen, C., Jiang, T., Yu, Z. & Guo, B. 2017 Waterbody information extraction from remote-sensing images after disasters based on spectral information and characteristic knowledge. *Int. J. Remote Sens.* **38** (5), 1404–1422.

Zhou, W., He, L., Ma, R., Liu, G. & Yuan, H. 2012 Extraction of water information based on LBV transformation of TM image using the object-oriented method. *J. Grad. Univ. Chin. Acad. Sci.* **29**, 775–779.

First received 12 May 2021; accepted in revised form 23 June 2021. Available online 29 July 2021